Journal Name

ARTICLE TYPE

Cite this: DOI: 10.1039/xxxxxxxxxx

Geometrical Flexibility of Platinum Nanoclusters: Impact on Catalytic Decomposition of Ethylene Glycol†

Mehdi Mahmoodinia,[a] Thuat T. Trinh,*[a,b] Per-Olof Åstrand,*[a] and Khanh-Quang Tran[c]

Received Date
Accepted Date

DOI: 10.1039/xxxxxxxxxx

www.rsc.org/journalname

Catalytic decomposition of ethylene glycol on the Pt_{13} cluster was studied as a model system for hydrogen production from lignocellulosic material. Ethylene glycol was chosen as a starting material because of two reasons, it is the smallest oxygenate with a 1:1 carbon to oxygen ratio and it contains the C–H, O–H, C–C, and C–O bonds also present in biomass. Density functional theory calculations were employed for predictions of reaction pathways for C–H, O–H, C–C and C–O cleavages, and Brønsted-Evans-Polanyi relationships were established between the final state and transition state for all mechanisms. The results show that Pt_{13} catalyzes the cleavage reactions of ethylene glycol more favourably than a Pt surface. The flexibility of Pt_{13} clusters during the reactions is the key factor in reducing the activation barrier. Overall, the results demonstrate that ethylene glycol and thus biomass can be efficiently converted into hydrogen using platinum nanoclusters as catalyst.

1 Introduction

Considering the possibility to get biomass-based fuels adapted to the existing infrastructure for energy production, of which more than 80% in the world are based on fossil fuel, biomass is one of the most promising renewable alternatives to fossil fuel[1–3]. Furthermore, renewable biomass can be converted to value-added chemicals and advanced fuels such as hydrogen for fuel-cell applications[4–6]. Traditionally, hydrogen can be produced from biomass via thermal gasification coupled with the water-gas shift reaction[7,8]. However, this process takes place at relatively high temperatures and produces gaseous impurities at the same time, which requires costly post-processing for fuel-cell applications. Alternatively, hydrogen can be produced from biomass via aqueous phase reforming (APR) of biomass-derived oxygenated compounds including carboxylic acids, aldehydes, ketones, alcohols, and phenols, which are commonly obtained from fast pyrolysis or liquefaction of biomass[1,2]. APR involves dehydrogenation, C–C bond cleavage, and the water-gas shift reaction[2]. In general, to maximize the production of hydrogen, it is desirable to maximize dehydrogenation and C–C bond cleavage while minimizing C–O bond breaking by using a suitable catalyst[9].

The catalytic decomposition of biomass-derived oxygenate has been studied using density functional theory (DFT)[10–12]. For this purpose, smaller oxygenates with a 1:1 carbon to oxygen ratio are particularly attractive[13] since unlike less oxygenated compounds derived from biomass, they do not require the addition of steam or oxygen to remove carbon from the metal in reforming processes[14]. Indeed, higher oxygenated species have higher catalytic reforming selectivity. It has been reported that the catalytic reforming selectivity of ethanol (less oxygenated) on bimetallic surface is lower than that of ethylene glycol (more oxygenated), particularly as the surface *d*-band center moves closer to the Fermi level[14]. This is presumably due to the fact that the binding energy of ethanol is too large, leading to total decomposition to atomic carbon and oxygen[14], instead of a reaction scheme through initial dehydrogenation and C–C bond scission to produce CO and H_2. This would require, at least in principle, the addition of steam or oxygen to remove the atomic carbon from the metal surface during the reforming process[13]. Ethylene glycol is the smallest oxygenate of this type, containing the C–H, O–H, C–C, and C–O bonds present in biomass. Therefore, ethylene glycol has been used extensively as model compound for studying the catalytic decomposition of biomass-derived oxygenates[5,9,10,13,14].

Platinum-based catalysts have been identified as a promising material for oxygenate conversion because of its combination of high reforming activity, synthesis gas product selectivity, and water-gas shift activity[15]. For example, platinum is an effec-

[a] *Department of Chemistry, Norwegian University of Science and Technology (NTNU), N-7491 Trondheim, Norway*
[b] *Department of Civil and Environmental Engineering, Norwegian University of Science and Technology (NTNU), N-7491 Trondheim, Norway*
[c] *Department of Energy and Process Engineering, Norwegian University of Science and Technology (NTNU), N-7491 Trondheim, Norway*
∗ *Corresponding author:*
E-mail address: per-olof.aastrand@ntnu.no (P.-O. Åstrand) and thuat.trinh@ntnu.no
† Electronic Supplementary Information (ESI) available: [Basis set study, Table of energetic and structural properties for adsorbed intermediates, Figure for adsorbed intermediates, and optimized cartesian coordinates of stable intermediates.]. See DOI: 10.1039/b000000x/

tive catalyst for APR of ethylene glycol because of its combined high dehydrogenation activity and high selectivity for C–C bond breaking [13]. Indeed, an efficient catalyst for APR cannot allow the subsequent methanation reactions, which consume hydrogen and decrease the hydrogen selectivity [16]. Pt- and Pd-based catalysts exhibit low rates for alkane production [16]. Furthermore, alloying Pt with other transition metals might reduce the cost of catalysts while maintaining or even increasing the catalytic activity and selectivity of ethylene glycol catalytic decomposition. For example, bimetallic PtNi, PtCo, and PtFe catalysts have higher turnover rates for hydrogen production than monometallic Pt catalysts, thereby more fraction of catalytic sites would be available for the APR of ethylene glycol [5]. Interestingly, the activity of Pt catalysts are structural sensitive, and the Pt(211) surface is more active than the Pt(111) surface for ethylene glycol conversion [9].

To the best of our knowledge, however, the catalytic activity of Pt clusters has not been investigated for this reaction. Cluster catalysts with very high ratio of the number of surface-to-bulk atoms are of significant interest in catalysis because they can act as individual active sites and small changes in their size and composition can potentially affect the activity and selectivity of a reaction [17,18]. For example, small ionic and neutral Pt clusters have been found to be excellent catalysts for the processes of (de)hydrogenation and cracking of alkanes [19–28]. The key reason for their high catalytic activity is the coordinative unsaturation [21]. A detailed understanding of the reaction mechanisms in biomass-derived molecules is a key factor to design an effective catalysts for biomass conversion. Hence, we examined the transition states of C–H, O–H, C–C, and C–O bond-cleaving reactions for $C_2H_xO_2$ dehydrogenation intermediates of ethylene glycol on Pt_{13}. DFT calculations of reaction pathways were employed in the gas phase assuming that the effect of solvation is negligible, an approximation based on that decomposition pathways of ethylene glycol in the gas phase were in excellent agreement with the bond scission sequence of deuterated ethylene glycols in solution using temperature-programmed desorption (TPD) experiments [13]. Our assumption is also in agreement with the recent DFT studies where indicated that the general trends for decomposition pathways of ethylene glycol is similar in both vapor and aqueous phases [29].

2 Computational details

All geometry optimizations of the molecular systems were carried out using DFT as implemented in the Amsterdam Density Functional (ADF) package [30,31]. The exchange-correlation part of the functional is described by the generalized gradient approximation (GGA) and the Perdew-Burke-Ernzerhof (PBE) functional [32]. A more recent dispersion correction proposed by Grimme with Becke-Johnson damping (DFT-D3-BJ) [33] is added to the functional to improve the description of weak interactions. Scalar relativistic effects are taken into account at the all-electron level within the zero-order-regular approximation approach [34–36], where its accuracy in treating heavy elements and in particular platinum has been assessed in several earlier publications [34–40]. The molecular orbitals were described by Slater-type basis functions of valence triple-ζ quality with one set of polarization function (TZP) [41], based on a basis set study (more information is available in the Supporting Information).

The transition state (TS) search and energy barriers of the elementary steps are calculated by the transition state reaction coordinate (TSRC) feature, as implemented in ADF, with convergence criteria of 1.0×10^{-4} and 5.0×10^{-3} au on the energy and the gradient, respectively. The TS search for a reaction on a cluster is more tricky than on a surface, due to the geometrical changes in the cluster structure during a reaction. Hence, for some of the transition states, a gradient threshold of 5.0×10^{-2} au has been applied, however, the deviation in the energy barriers with this criterion is less than 0.02 eV.

Vibrational frequency analysis is performed in order to confirm the existence of only one imaginary frequency for the mode in the direction of the reaction coordinate for each transition state. The activation energy, E_a, is the energy difference between transition state and adsorbed initial state. The reaction energy, ΔE, is calculated as the energy difference between the final state and the initial state.

3 Results and Discussions

3.0.0.1 Pt_{13} Clusters: Prior to studying the ethylene glycol decomposition on Pt_{13}, we examined several different structures of Pt_{13}, including cuboctahedron (fcc), distorted cuboctahedron (D_{4h}), icosahedron (ico), truncated decahedron (D_{5h}), hexagonal building unit (hcp), and a structure with C_{2v} symmetry (C_{2v}), which were optimized without constraints to find the most stable configuration. It turns out that the deformed structure with C_{2v} symmetry shows the largest stability followed by the D_{4h} structure. Local optimizations were done with different spin multiplicities (2S+1, i.e. S = 0, 1, 2, 3, and 4) for the C_{2v} structure to find the ground state. The triplet state is found to be the electronic ground state and the singlet state is slightly higher by 32 meV. The relative energies of all configurations with respect to the energy of the C_{2v} configuration, $E_{tot}^{C_{2v}}$, are calculated as

$$E_{rel} = E_{tot}^{cluster} - E_{tot}^{C_{2v}} \quad (1)$$

where $E_{tot}^{cluster}$ is electronic ground state energy, triplet, of a particular configuration. The results are shown in Figure 1. A positive

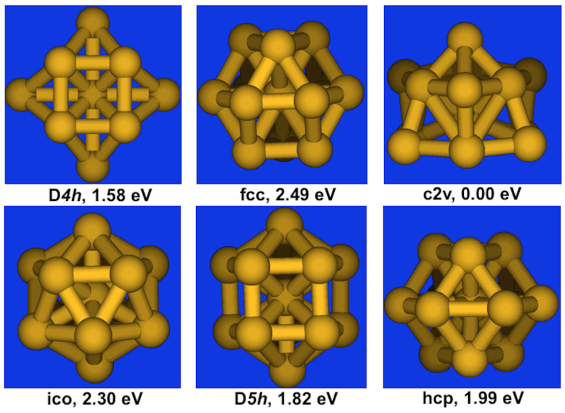

Fig. 1 Optimized geometries for different Pt_{13} clusters and their relative stability, E_{rel}.

Table 1 Energetics and Structural Information for C–H Bond-Cleaving Transition States of $C_2H_xO_2$ Intermediates of Ethylene Glycol on Pt_{13}[a].

					Pt_{13} deformation (eV)		
elementary reactions	E_a [eV]	ΔE [eV]	C–H [Å]	TS labels	React.	Trans.	Prod.
$CH_2OH\text{-}CH_2OH^* + * \longrightarrow CHOH\text{-}CH_2OH^* + H^*$	0.83	–0.74	1.40	TS1a	0.78	0.95	0.79
$CHOH\text{-}CH_2OH^* + * \longrightarrow COH\text{-}CH_2OH^* + H^*$	0.67	–0.13	1.45		0.58	0.63	1.06
$CHOH\text{-}CH_2OH^* + * \longrightarrow CHOH\text{-}CHOH^* + H^*$	0.69	–0.50	1.44		0.58	1.48	1.00
$CH_2OH\text{-}CH_2O^* + * \longrightarrow CH_2OH\text{-}CHO^* + H^*$	0.08	–0.14	1.70	TS2b	0.89	0.81	0.54
$CH_2OH\text{-}CH_2O^* + * \longrightarrow CHOH\text{-}CH_2O^* + H^*$	0.71	–0.30	1.47		0.89	0.56	0.92
$CHOH\text{-}CHOH^* + * \longrightarrow CHOH\text{-}COH^* + H^*$	0.74	–0.89	1.51		1.18	0.91	0.84
$CHOH\text{-}CH_2O^* + * \longrightarrow CHOH\text{-}CHO^* + H^*$	0.32	–0.89	1.37	TS3a	0.89	0.40	1.04
$CHOH\text{-}CH_2O^* + * \longrightarrow COH\text{-}CH_2O^* + H^*$	0.62	–0.06	1.59		0.89	0.90	1.14
$CH_2OH\text{-}CHO^* + * \longrightarrow CH_2OH\text{-}CO^* + H^*$	0.62	–0.79	1.42	TS3b	0.81	0.81	0.40
$CH_2OH\text{-}CHO^* + * \longrightarrow CHOH\text{-}CHO^* + H^*$	0.99	–0.96	1.40		0.81	0.62	0.58
$CH_2OH\text{-}CO^* + * \longrightarrow CHOH\text{-}CO^* + H^*$	0.60	–0.66	1.46		1.04	0.36	1.22
$CHOH\text{-}COH^* + * \longrightarrow COH\text{-}COH^* + H^*$	0.38	–0.38	1.46		1.37	1.27	1.71
$CHOH\text{-}CHO^* + * \longrightarrow COH\text{-}CHO^* + H^*$	0.86	0.07	1.47		1.04	0.94	0.66
$CHOH\text{-}CHO^* + * \longrightarrow CHOH\text{-}CO^* + H^*$	0.23	–0.50	1.40	TS4a	1.04	0.50	0.67
$CHOH\text{-}CO^* + * \longrightarrow COH\text{-}CO^* + H^*$	0.65	–0.41	1.41	TS5a	1.15	1.24	1.30
$CH_2O\text{-}CO^* + * \longrightarrow CHO\text{-}CO^* + H^*$	0.13	–0.37	1.51	TS5c	0.83	0.64	0.99
$CHO\text{-}CO^* + * \longrightarrow CO\text{-}CO^* + H^*$	0.66	–0.34	1.38	TS6b	1.10	0.72	0.86

[a] E_a is the activation barrier (change in electronic energy from initial state to transition state). ΔE is the change in electronic energy of reaction (all reactants and products adsorbed on separate clusters). TS labels represent the labels of the transition states which are shown in the energy diagram in Figure 2. The last three columns show the Pt_{13} deformation energy in the reactants, transitions states, and the products during each elementary step.

Table 2 Energetics and Structural Information for O–H Bond-Cleaving Transition States of $C_2H_xO_2$ Intermediates of Ethylene Glycol on Pt_{13}. The column headings in this Table are the same as in Table 1.

					Pt_{13} deformation (eV)		
elementary reactions	E_a [eV]	ΔE [eV]	O–H [Å]	TS labels	React.	Trans.	Prod.
$CH_2OH\text{-}CH_2OH^* + * \longrightarrow CH_2OH\text{-}CH_2O^* + H^*$	0.10	–0.51	1.43	TS1b	0.78	0.91	0.96
$CHOH\text{-}CH_2OH^* + * \longrightarrow CHO\text{-}CH_2OH^* + H^*$	0.86	0.05	1.41		0.58	1.11	0.96
$CHOH\text{-}CH_2OH^* + * \longrightarrow CHOH\text{-}CH_2O^* + H^*$	0.52	–0.20	1.45	TS2a	0.58	0.97	1.00
$CH_2OH\text{-}CH_2O^* + * \longrightarrow CH_2O\text{-}CH_2O^* + H^*$	0.51	0.01	1.68		0.89	0.95	0.97
$CHOH\text{-}CHOH^* + * \longrightarrow CHO\text{-}CHOH^* + H^*$	0.56	–0.18	1.35		1.17	1.14	1.24
$CHOH\text{-}CH_2O^* + * \longrightarrow CHO\text{-}CH_2O^* + H^*$	0.90	0.19	1.43		0.89	0.92	0.34
$CH_2OH\text{-}CHO^* + * \longrightarrow CH_2O\text{-}CHO^* + H^*$	0.76	0.06	1.50		0.81	0.88	1.07
$CH_2OH\text{-}CO^* + * \longrightarrow CH_2O\text{-}CO^* + H^*$	0.36	–0.73	1.58	TS4b	1.04	0.35	0.52
$CHOH\text{-}COH^* + * \longrightarrow CHOH\text{-}CO^* + H^*$	0.00	–0.42	1.29		1.37	1.08	1.30
$CHOH\text{-}COH^* + * \longrightarrow CHO\text{-}COH^* + H^*$	0.31	0.06	1.37		1.37	1.30	1.14
$CHOH\text{-}CHO^* + * \longrightarrow CHO\text{-}CHO^* + H^*$	0.46	0.02	1.51		1.04	0.67	0.75
$CHOH\text{-}CO^* + * \longrightarrow CHO{-}CO^* + H^*$	0.56	–0.17	1.35	TS5b	1.15	0.99	0.93
$COH\text{-}CO^* + * \longrightarrow CO\text{-}CO^* + H^*$	0.65	–0.19	1.26	TS6a	1.38	1.19	1.18

value of E_{rel} indicates a less stable Pt_{13} cluster compared to C_{2v} configuration. Hence, we selected the C_{2v} structure for studying the ethylene glycol decomposition on Pt_{13}.

3.1 Adsorbed $C_2H_xO_2$ Intermediates on Pt_{13} Clusters

For the adsorbed intermediates, geometry optimization has been carried out with different spin multiplicities to find the electronic ground state. For intermediates with even (odd) number of hydrogens, the triplet (quartet) state is found to be the electronic ground state. The optimized geometries for the most stable intermediates of ethylene glycol at each level of dehydrogenation on Pt_{13} are shown in Figure S2. The adsorption energy of ethylene glycol on Pt_{13} is calculated to −0.52 eV, which is more favorable than on the Pt(111) surface (−0.37 eV) [13]. For this structure, ethylene glycol binds to the atop sites of the Pt_{13} cluster through both oxygen atoms. Dehydrogenated intermediates of ethylene glycol bind to the Pt_{13} cluster via under-coordinated C and O atoms. Further information on the energetic and structural properties of these intermediates including the energy of adsorption (ΔE_{ads}) and bond lengths are given in Table S1.

3.2 Decomposition Reactions of $C_2H_xO_2$ Species on Pt_{13} Clusters

The dehydrogenation of ethylene glycol on Pt_{13} begins through a rapid O–H bond scission with the activation barrier and reaction energy of 0.10 and –0.51 eV, respectively. The energy

Table 3 Energetics and Structural Information for C–C Bond-Cleaving Transition States of $C_2H_xO_2$ Intermediates of Ethylene Glycol on Pt_{13}. The column headings in this Table are the same as in Table 1.

					Pt_{13} deformation (eV)		
elementary reactions	E_a [eV]	ΔE [eV]	C–C [Å]	TS labels	React.	Trans.	Prod.
$CH_2OH\text{-}CH_2OH^* + * \longrightarrow 2CH_2OH^*$	2.64*	–0.89	1.90		0.78	1.31	0.70
$CHOH\text{-}CH_2OH^* + * \longrightarrow CHOH^* + CH_2OH^*$	2.09	0.20	2.04		0.58	1.00	1.14
$CH_2OH\text{-}CH_2O^* + * \longrightarrow CH_2OH^* + CH_2O^*$	1.77	–0.05	2.08		0.89	1.04	1.02
$CHOH\text{-}CHOH^* + * \longrightarrow 2CHOH^*$	1.07	–0.77	2.25		1.18	0.84	0.77
$CHOH\text{-}CH_2O^* + * \longrightarrow CHOH^* + CH_2O^*$	1.25	–0.05	2.06		0.89	0.80	0.97
$CH_2OH\text{-}CHO^* + * \longrightarrow CH_2OH^* + CHO^*$	1.11	–0.46	2.07		0.81	0.69	0.66
$CH_2OH\text{-}CO^* + * \longrightarrow CH_2OH^* + CO^*$	0.76	–139	2.02		1.04	0.33	0.45
$CHOH\text{-}COH^* + * \longrightarrow CHOH^* + COH^*$	0.81	–0.59	2.04		1.37	1.19	1.62
$CHOH\text{-}CHO^* + * \longrightarrow CHOH^* + CHO^*$	0.94	–0.34	1.92		1.04	0.57	0.59
$CHOH\text{-}CO^* + * \longrightarrow CHOH^* + CO^*$	0.38	–1.17	1.98		1.15	0.96	1.54
$CH2O\text{-}CO^* + * \longrightarrow CH2O^* + CO^*$	0.70	–0.67	2.26		0.83	0.03	1.41
$COH\text{-}CO^* + * \longrightarrow COH^* + CO^*$	0.55	–1.19	1.87		1.38	1.01	1.35
$CHO\text{-}CO^* + * \longrightarrow CHO^* + CO^*$	0.45	–1.12	1.96		1.02	1.07	1.27
$CO\text{-}CO^* + * \longrightarrow 2CO^*$	0.09	–2.63	1.96	TS7	1.29	1.13	1.10

* After several attempts this TS is not completely converged.

Table 4 Energetics and Structural Information for C–O Bond-Cleaving Transition States of $C_2H_xO_2$ Intermediates on Pt_{13}. The column headings in this Table are the same as in Table 1.

				Pt_{13} deformation (eV)		
elementary reactions	E_a [eV]	ΔE [eV]	C–O [Å]	React.	Trans.	Prod.
$CH_2OH\text{-}CH_2OH^* + * \longrightarrow CH_2OH\text{-}CH_2{}^* + OH^*$	1.10	–1.03	2.08	0.78	0.16	0.96
$CHOH\text{-}CH_2OH^* + * \longrightarrow CH\text{-}CH_2OH^* + OH^*$	1.05	–0.36	2.23	0.58	0.82	0.69
$CHOH\text{-}CH_2OH^* + * \longrightarrow CHOH\text{-}CH_2^* + OH^*$	1.19	–0.54	2.16	0.58	0.92	0.73
$CH_2OH\text{-}CH_2O^* + * \longrightarrow CH_2\text{-}CH_2O^* + OH^*$	1.27	–0.34	2.28	0.89	0.80	0.83
$CHOH\text{-}CHOH^* + * \longrightarrow CH\text{-}CHOH^* + OH^*$	2.37*	0.16	2.64	1.18	1.73	1.02
$CHOH\text{-}CH_2O^* + * \longrightarrow CH\text{-}CH_2O^* + OH^*$	0.68	–0.13	2.37	0.89	0.58	0.81
$CH_2OH\text{-}CHO^* + * \longrightarrow CH_2\text{-}CHO^* + OH^*$	1.25	0.11	2.13	0.81	0.45	1.10
$CH_2OH\text{-}CO^* + * \longrightarrow CH_2\text{-}CO^* + OH^*$	1.28	–0.86	1.90	1.04	0.46	1.19
$CHOH\text{-}COH^* + * \longrightarrow CHOH\text{-}C^* + OH^*$	1.07	0.32	2.25	1.37	1.12	2.07
$CHOH\text{-}COH^* + * \longrightarrow CH\text{-}COH^* + OH^*$	0.62	–0.78	2.04	1.37	1.23	1.32
$CHOH\text{-}CHO^* + * \longrightarrow CH\text{-}CHO^* + OH^*$	0.96	–0.20	2.41	1.04	0.60	1.38
$CHOH\text{-}CO^* + * \longrightarrow CH\text{-}CO^* + OH^*$	0.84	–0.52	2.53	1.15	0.83	1.11
$COH\text{-}CO^* + * \longrightarrow C\text{-}CO^* + OH^*$	1.04	-0.42	2.07	1.38	1.06	1.29

* After several attempts this TS is not completely converged.

barrier of initial C–H bond breaking of ethylene glycol is calculated to 0.83 eV, with a reaction energy of –0.74 eV. The C–C and C–O bond breaking of ethylene glycol are both energetically and thermodynamically not favorable compared to the dehydrogenation reactions. Therefore, both the $CHOH-CH_2OH$ and CH_2OH-CH_2O are the most favorable intermediates resulting from initial decomposition of ethylene glycol on Pt_{13}. The energetic information and transition state bond distances for C–H, O–H, C–C, and C–O bond-cleaving reactions of ethylene glycol intermediates are reported in Tables 1–4, respectively.

For the $C_2H_5O_2$ species, 12 elementary steps including C–H, O–H, C–C, and C–O bond-breaking reactions, may be involved in the decomposition of the $CHOH-CH_2OH$ and CH_2OH-CH_2O intermediates. For decomposition of the CH_2OH-CH_2O intermediate, the C–H bond scission to form the $CH_2OH-CHO$ intermediate is found to be the most favorable reaction intermediate with a barrier of 0.08 eV and reaction energy of –0.14 eV, respectively. The decomposition of $CHOH-CH_2OH$ proceeds through the O–H bond scission to $CHOH-CH_2O$ with a barrier of 0.52 eV and reaction energy of –0.20 eV, respectively, in competition with the C–H bond scission reactions to form $COH-CH_2OH$ and $CHOH-CHOH$ with the activation barriers of 0.67 and 0.69 eV, respectively. However, formation of $CHOH-CHOH$ with reaction energy of –0.50 eV is thermodynamically more favorable (Tables 1 and 2). Hence, the $CHOH-CH_2O$, $CH_2OH-CHO$, and $CHOH-CHOH$ intermediates are selected for further analysis in the next step of the decomposition.

There are 14 elementary steps that may be involved in the decomposition of the $C_2H_4O_2$ species. The lowest transition state is for C–H cleaving of $CHOH-CH_2O$ to form $CHOH-CHO$ with a barrier and reaction energies of 0.32 and –0.89 eV, respectively. The barrier of 0.62 eV for C–H bond cleavage of

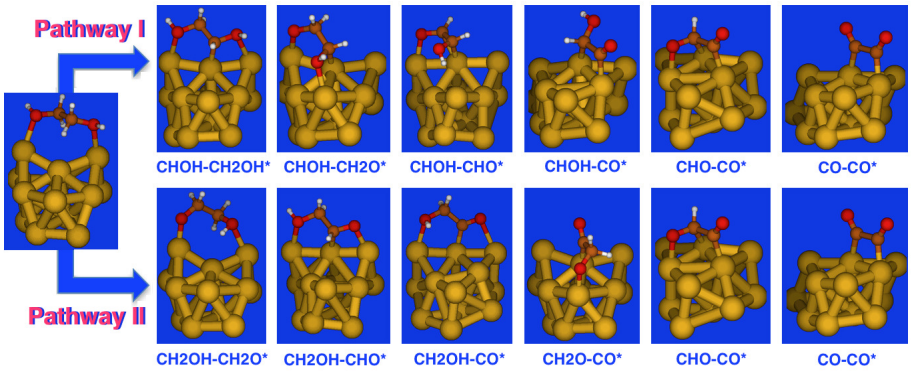

Fig. 2 Stable intermediates for two ethylene glycol dehydrogenation pathways on Pt_{13} cluster. Pathways I and II represent the intermediates decomposed via initial C–H and O–H bond-cleaving reactions, respectively. Pt, C, O, and H atoms are represented by the yellow, brown, red, and white circles, respectively. An energy diagram is presented in Figure 3, and the relative energies are given in Table 5.

$CH_2OH-CHO$ to form CH_2OH-CO is comparable with that of $CHOH-CH_2O$ to form $COH-CH_2O$ and of CHOH−CHOH to form CHOH−COH, respectively, however, the thermodynamics for formation of CH_2OH-CO and CHOH−COH are significantly more favorable and are exothermic by 0.79 and 0.89 eV, respectively (Tables 1 and 2).

Among 15 elementary reactions that have been considered for decomposition of the $C_2H_3O_2$ species, the lowest activation barriers are for O–H bond cleavages of CHOH−COH and CH_2OH-CO to form CHOH−CO and CH_2O-CO with the corresponding barriers of 0.00 and 0.36 eV, respectively, together with a C–H bond cleavage of CHOH−CHO to form CHOH−CO with an activation barrier of 0.23 eV. The formation of CHO−COH from the O–H bond cleavage of CHOH−COH intermediate has also a considerably lower barrier (0.31 eV), however, in competition with the formation of CHOH−CO, it is both kinetically and thermodynamically less favorable (Tables 1 and 2).

The decomposition of the $C_2H_2O_2$ species have been considered using 6 elementary steps, and the lowest barriers for dehydrogentation of these intermediates are found for the C–H bond scission of CH_2O-CO to form CHO−CO, followed by formation of this intermediate through the O–H bond cleavage of CHOH−CO with the activation energies of 0.13 and 0.56 eV, respectively. The thermodynamics of these two elementary reactions are exothermic by 0.37 and 0.17 eV, respectively. The C–C bond-breaking of $C_2H_2O_2$ species are favorable enough to be competitive with the dehydrogenation reactions (Tables 3). The activation barrier for the C–C bond scission of CHOH−CO is calculated to 0.38 eV and it is exothermic by 1.17 eV. However, the activation barriers for the C–O bond-breakings are still significantly higher than the dehydrogenation and the C–C bond-breaking reactions.

For highly dehydrogenated intermediates, the C–C bond-breaking reaction are both kinetically and thermodynamically more facile than the dehydrogenation reactions. The activation barriers for C–C bond scission of CHO−CO and COH−CO are calculated to 0.45 and 0.55 eV, respectively, which are slightly lower than those of the dehydrogenation reactions (0.66 and 0.65 eV, respectively), indicating that these elementary steps have comparable rates. However, the corresponding C–C bond scissions are highly exothermic by 1.12 and 1.19 eV, respectively. The C–O bond-breaking barriers are still significantly higher than the dehydrogenation and the C–C bond scission reactions (Tables 3 and 4).

The CO–CO intermediate has very low activation barrier (0.09 eV) for C–C bond-cleaving reaction and will quickly decompose to two CO molecule on the surface of Pt_{13}. This reaction is highly exothermic with reaction energy of –2.63 eV (Table 3).

3.3 Geometrical Flexibility of Pt_{13}

Figure 2 briefly depicts the evolution of the $C_2H_xO_2/Pt_{13}$ system during two reaction pathways via C–H and O–H cleavages, respectively. These are two main competitive pathways after the initial O–H or C–H bond scission. The intermediates of ethylene glycol following these pathways are similar for Pt_{13} and the Pt surface[13] in the sense that it is the same reactions taking place, the main difference being that Pt_{13} dynamically reshape during the reaction. The average bond distances of Pt–Pt in the bare Pt_{13} cluster is 2.59 Å. However, in some transition states, the Pt–Pt bond is elongated by more than 0.6 Å during the bond scission reaction. For example, during the C–H bond-cleaving reaction, a Pt–Pt bond distance for the outermost Pt shells in the transition state is calculated to 3.21 Å, where the deformation energy of the Pt_{13} cluster is calculated to 0.95 eV. In addition, a high geometry adoption is found for the TS4a transition state, where a Pt–Pt bond is calculated to 3.39 Å, while its energy barrier is small (0.23 eV). The energy evolution of the Pt_{13} cluster along the C–H, O–H, C–C, and C–O bond-cleaving reactions are presented in Tables 1, 2, 3, and 4, respectively. It is indeed interesting to see that along the reaction, the energy of Pt_{13} alone can differ by as much as 0.86 eV, so the geometry of Pt_{13} adapt extensively to the reaction and hence lower the activation barriers. The thermodynamic stability of the global and low-lying minima for Pt_{10-13} clusters have recently been investigated using DFT calculations[42]. The results demonstrated a high degree of fluxionality for the Pt_{11-13} clusters which provide insights into the high catalytic activity of Pt_{13} clusters.

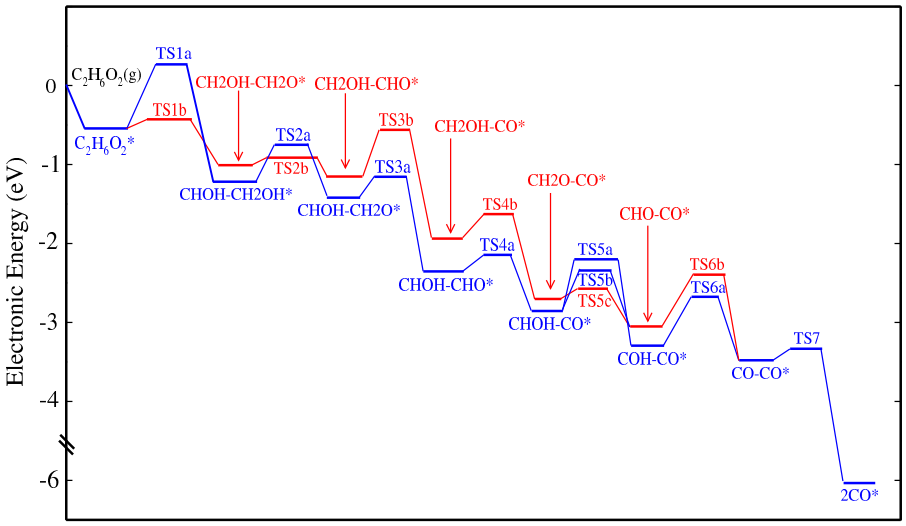

Fig. 3 Energy diagram for two ethylene glycol decomposition pathways. The blue line shows the pathway through initial C–H bond scission. The red line shows the pathway from initial O–H bond scission. All values shown are with respect to gas-phase ethylene glycol, an unperturbed Pt_{13} cluster and all excess hydrogen atoms adsorbed separately. Relative energies and transition state labels are provided in Table 5.

Table 5 Relative Energy Corresponding to Figure 3 for the Intermediates (Int.) and Transition States (TS) Involved in the Decomposition Pathways of Ethylene Glycol on Pt_{13}.[a]

intermediate or transition state	relative energy Int.	relative energy TS	TS labels
CH_2OH-CH_2OH (g) + ∗	0.00	—	—
$CH_2OH-CH_2OH^*+*\longrightarrow CHOH-CH_2OH^*+H^*$	–0.52	0.31	TS1a
$CH_2OH-CH_2OH^*+*\longrightarrow CH_2OH-CH_2O^*+H^*$	–0.52	–0.42	TS1b
$CHOH-CH_2OH^*+*\longrightarrow CHOH-CH_2O^*+H^*$	–1.25	–0.73	TS2a
$CH_2OH-CH_2O^*+*\longrightarrow CH_2OH-CHO^*+H^*$	–1.02	–0.94	TS2b
$CHOH-CH_2O^*+*\longrightarrow CHOH-CHO^*+H^*$	–1.46	–1.14	TS3a
$CH_2OH-CHO^*+*\longrightarrow CH_2OH-CO^*+H^*$	–1.17	–0.55	TS3b
$CHOH-CHO^*+*\longrightarrow CHOH-CO^*+H^*$	–2.35	–2.11	TS4a
$CH_2OH-CO^*+*\longrightarrow CH_2O-CO^*+H^*$	–1.96	–1.60	TS4b
$CHOH-CO^*+*\longrightarrow COH-CO^*+H^*$	–2.84	–2.20	TS5a
$CHOH-CO^*+*\longrightarrow CHO-CO^*+H^*$	–2.84	–2.28	TS5b
$CH_2O-CO^*+*\longrightarrow CHO-CO^*+H^*$	–2.69	–2.57	TS5c
$COH-CO^*+*\longrightarrow CO-CO^*+H^*$	–3.25	–2.61	TS6a
$CHO-CO^*+*\longrightarrow CO-CO^*+H^*$	–3.02	–2.36	TS6b
$CO-CO^*+*\longrightarrow 2CO^*$	–3.44	–3.36	TS7

[a] Electronic energies (eV) of intermediates and transition states are with respect to gas-phase ethylene glycol, an unperturbed Pt_{13} cluster and all excess hydrogen atoms adsorbed separately.

3.4 Energy Diagram

An energy diagram of the two possible decomposition pathways including the most stable intermediates and the transition states is presented in Figure 3. The electronic energies corresponding to these intermediates and transition states are calculated with respect to gas-phase ethylene glycol, an unperturbed Pt_{13} cluster (see Table 5). The optimized structures for all stable intermediates are depicted in Figure S2.

The reaction along both C–H and O–H bond scission are thermodynamically favorable with decreasing reaction enthalpy. The decomposition of ethylene glycol begins with a rapid O–H bond scission through TS1b (see Figure 3 and Table 2) and proceeds via sequential hydrogen elimination to from alkoxide intermediates. This is consistent with the typical reaction sequence of alcohol decomposition on group VIII metals which proceeds through an alkoxide formation[9,43,44]. The pathway through α–H elimination has higher activation barriers for the first (TS1a) and the second (TS2a) elementary reaction steps (see Figure 3 and Table 1), however, after that the pathway through initial C–H bond scission (blue diagram in Figure 3) is preferred, which is in accordance with the reactions on the Pt surface[13]. The TPD experiments with deuterated ethylene glycol also confirmed these bond scission sequences for ethylene glycol decomposition on the Pt surface[13].

3.5 Energy Barriers

Comparing the energy barriers of transition states gives an understanding of the kinetics for ethylene glycol decomposition. Figure 4 shows the activation barriers of the competing C–H, O–H, and C–C bond breaking reactions for ethylene glycol intermediates on Pt_{13} as a function of the number of hydrogen atoms. The barriers for C–H and O–H bond scission are low in all elementary steps of the dehydrogenation process. In contrast, the barriers for C–C bond breaking are very high at the early steps of dehydrogenation (in the range of 1.5–2.6 eV), and as intermediates become more dehydrogenated, the C–C bond scission becomes both thermodynamically and kinetically more facile than dehydrogenation, which is reflected by the strong binding of the CO molecule to Pt_{13}. Our results therefore strengthen the preferred mechanism which suggests that the decomposition pathway of ethylene glycol over Pt proceeds first through dehydrogenation to reach an intermediate with one terminal CO, followed by C–C bond cleavage[9,13].

The activation barriers for C–O bond-cleaving reactions over Pt_{13} cluster are relatively high compared with the dehydrogenation and C–C bond-breaking reactions, indicating a low selectivity toward products from C–O bond cleavage. This is in agreement

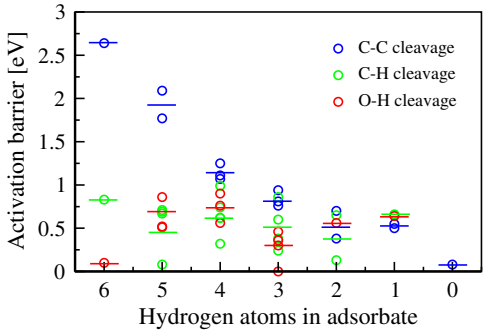

Fig. 4 The C–H, O–H, and C–C activation barriers of $C_2H_xO_2$ intermediates on Pt_{13} as a function of hydrogen atoms in each species. Average value of each level of dehydrogenation is denoted with a horizontal dash.

with studies of ethylene glycol decomposition on Pt and Ni/Pt surfaces[9,13,45]. The results imply that decomposition reactions on Pt_{13} has lower activation barriers and more favorable reaction enthalpies compared to the Pt surface[9].

3.6 BEP Relationships for Barrier Prediction

Brønsted-Evans-Polanyi (BEP) relationships[46–48] are powerful to predict transition state energies and reaction barriers, and have been applied to heterogeneous catalysis reactions extensively[49–54]. We derived BEP relationships based on the calculated transition state energies and reaction enthalpies of the elementary steps involved in the decomposition of ethylene glycol on Pt_{13} (see Tables 1–4). The elementary steps are defined in the exothermic direction. The transition state (E_{TS}) and final state (E_{FS}) energies are given relative to the energies of the gas-phase reactants in each elementary step. Figure 5 shows that there is a good linear relation for both C–H/O–H and C–C/C–O bond scission reactions, respectively. The slope of the BEP interpolation line is a measure of the earliness or lateness of the transition state[51,53], in the way that a near-zero value indicates an early transition state, whereas a near-unity value indicates a late transition state. The slope of the BEP relations for the C–H/O–H and C–C/C–O bond scission reactions are calculated to 0.98 and 1.08, respectively, indicating that the general trend for these transition states on Pt_{13} are that they are late (written in the exothermic direction). However, the intercept of the BEP relations vary from one reaction to another, for example, the intercept for the C–H/O–H (0.44 eV) relation is much lower than that for the C–C/C–O (1.67 eV) relation, which may represent the differences in the transition state energies of these processes. The standard error of the BEP relations for the C–H/O–H and C–C/C–O bond scission reactions are calculated as 0.26 and 0.51 eV, respectively.

4 Conclusion

We have established mechanisms for C–H, O–H, C–C, and C–O cleavage of ethylene glycol, as the simplest representative of biomass-derived polyols, on Pt_{13} using DFT calculations. It is found that the decomposition of ethylene glycol begins with a rapid O–H bond scission to from an alkoxide intermediate and

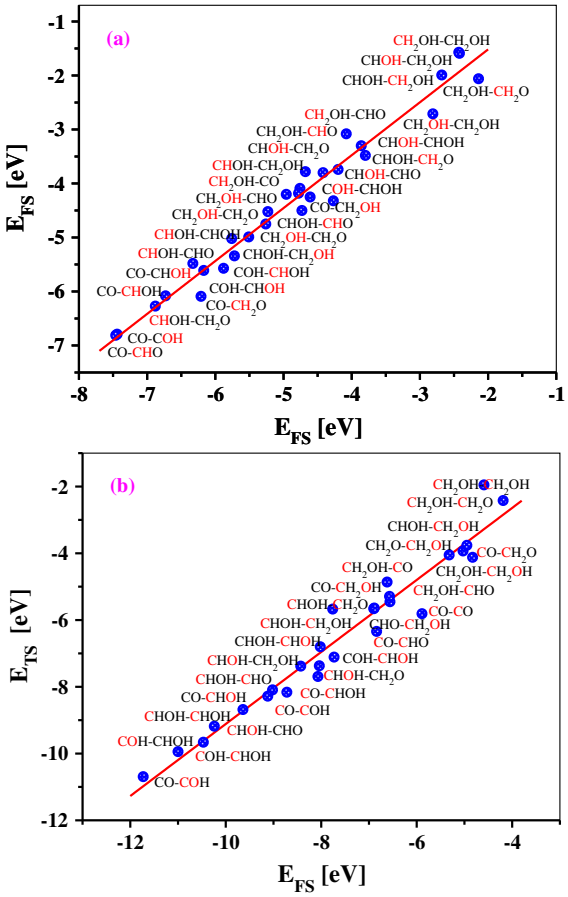

Fig. 5 (a) BEP relationships for the C–H/O–H bond scission reactions. Final state (E_{FS}) and transition state (E_{TS}) energies are relative to initial-state gas-phase energies, where each corresponding surface reaction is represented in the exothermic direction. The linear regression equation is E_{TS} [eV] = 0.98 E_{FS} [eV] + 0.44 [eV]. (b) BEP relationships for the C–C/C–O bond scission reactions. The linear regression equation is E_{TS} [eV] = 1.08 E_{FS} [eV] + 1.67 [eV]. The standard error of the BEP relations for the C–H/O–H and C–C/C–O bond-breaking reactions are calculated to 0.26 and 0.51 eV, respectively. Colored letters indicate the bonds to be broken.

then proceeds via sequential α–H elimination, which is consistent with the typical reaction sequence of alcohol decomposition on group VIII metals[9,43]. Cleavage of the C–C bond in ethylene glycol has a very high barrier at the early stage of dehydrogenation but as intermediates become more dehydrogenated, the C–C bond-breaking becomes more facile than dehydrogenation. Hence, our results strengthen the preferred mechanism for bond-breaking sequence of ethylene glycol over Pt which suggests that the decomposition proceeds first through dehydrogenation to reach an intermediate with one terminal CO, followed by C–C bond cleavage[9,13]. A low selectivity toward products from C–O bond cleavage is observed. The results imply that the Pt_{13} cluster is a more efficient catalyst for ethylene glycol conversion to hydrogen with lower activation barriers and a more favorable reaction enthalpy than the Pt surface. The geometrical flexibility of a platinum cluster adapting to the reaction steps is the key point in this difference. BEP relations to predict activation barriers for the C–H/O–H and C–C/C–O scission reactions have also been es-

tablished.

5 Acknowledgment

This work is a part of the ISP project (209337) with financial support from the Norwegian Research Council. Computational time provided by the Notur project (account nn2920k and nn9229k) is acknowledged.

References

1 R. D. Cortright, R. R. Davda and J. A. Dumesic, *Nature*, 2002, **418**, 964–967.
2 G. W. Huber, S. Iborra and A. Corma, *Chem. Rev.*, 2006, **106**, 4044–4098.
3 E. L. Kunkes, D. A. Simonetti, R. M. West, J. C. Serrano-Ruiz, C. A. Gärtner and J. A. Dumesic, *Science*, 2008, **322**, 417–421.
4 J. W. Shabaker, R. R. Davda, G. W. Huber, R. D. Cortright and J. A. Dumesic, *J. Catal.*, 2003, **215**, 344–352.
5 G. W. Huber, J. W. Shabaker, T. E. Steven and J. A. Dumesic, *Appl. Catal., B*, 2006, **62**, 226–235.
6 G. Wen, Y. Xu, H. Ma, Z. Xu and Z. Tian, *Int. J. Hydrogen Energy*, 2008, **33**, 6657–6666.
7 T. A. Milne, C. C. Elam and R. J. Evans, *Hydrogen from Biomass: State of the Art and Research Challenges; TOPICAL*, National Renewable Energy Lab., Golden, CO (United States) Report IEA-H–2-TR-02/001, 2002.
8 M. Balat, *Energy Sources, Part A*, 2010, **32**, 1388–1398.
9 X.-K. Gu, B. Liu and J. Greeley, *ACS Catal.*, 2015, **5**, 2623–2631.
10 J. Greeley and M. Mavrikakis, *J. Am. Chem. Soc.*, 2002, **124**, 7193–7201.
11 J. Greeley and M. Mavrikakis, *J. Am. Chem. Soc.*, 2004, **126**, 3910–3919.
12 S. Kandoi, J. Greeley, M. A. Sanchez-Castillo, S. T. Evans, A. A. Gokhale, J. A. Dumesic and M. Mavrikakis, *Top. Catal.*, 2006, **37**, 17–28.
13 M. Salciccioli, W. Yu, M. A. Barteau, J. G. Chen and D. G. Vlachos, *J. Am. Chem. Soc.*, 2011, **133**, 7996–8004.
14 O. Skoplyak, M. A. Barteau and J. G. Chen, *Catal. Today*, 2009, **147**, 150–157.
15 R. R. Davda, J. W. Shabaker, G. W. Huber, R. D. Cortright and J. A. Dumesic, *Appl. Catal., B*, 2005, **56**, 171–186.
16 R. R. Davda, J. W. Shabaker, G. W. Huber, R. D. Cortright and J. A. Dumesic, *Appl. Catal., B*, 2003, **43**, 13–26.
17 E. C. Tyo and S. Vajda, *Nat. Nanotechnol*, 2015, **10**, 577–588.
18 F. Dong, S. Heinbuch, Y. Xie, J. J. Rocca, E. R. Bernstein, Z.-C. Wang, K. Deng and S.-G. He, *J. Am. Chem. Soc.*, 2008, **130**, 1932–1943.
19 R. Burchand and L. C. Garla, *J. Catal.*, 1981, **71**, 360–372.
20 D. J. Trevor, R. L. Whetten, D. M. Cox and A. Kaldor, *J. Am. Chem. Soc.*, 1985, **107**, 519–521.
21 D. J. Trevor, D. M. Cox and A. Kaldor, *J. Am. Chem. Soc.*, 1990, **112**, 3742–3749.
22 U. Achatz, C. Berg, S. Joos, B. S. Fox, M. K. Beyer, G. Niedner-Schatteburg and V. E. Bondybey, *Chem. Phys. Lett.*, 2000, **320**, 53–58.
23 K. Koszinowski, D. Schröder and H. Schwarz, *J. Phys. Chem. A*, 2003, **107**, 4999–5006.
24 G. Kummerlöwe, I. Balteanu, Z. Sun, O. P. Balaj, V. E. Bondybey and M. K. Beyer, *Int. J. Mass Spectrom.*, 2006, **254**, 183–188.
25 C. Adlhart and E. Uggerud, *Chem. Commun.*, 2006, 2581–2582.
26 C. Adlhart and E. Uggerud, *Chem. Eur. J.*, 2007, **13**, 6883–6890.
27 S. Vajda, M. J. Pellin, J. P. Greeley, C. L. Marshall, L. A. Curtiss, G. A. Ballentine, J. W. Elam, S. Catillon-Mucherie, P. C. Redfern, F. Mehmood and *et al.*, *Nat. Mater.*, 2009, **8**, 213–216.
28 J. Dadras, E. Jimenez-Izal and A. N. Alexandrova, *ACS Catal.*, 2015, **5**, 5719–5727.
29 M. Faheem, M. Saleheen, J. Luac and A. Heyden, *Catal. Sci. Technol.*, 2016, **6**, 8242–8256.
30 C. F. Guerra, J. G. Snijders, G. te Velde and E. J. Baerends, *Theor. Chem. Acc.*, 1998, **99**, 391–403.
31 G. te Velde, F. M. Bickelhaupt, E. J. Baerends, C. F. Guerra, S. J. A. van Gisbergen, J. G. Snijders and T. Ziegler, *J. Comput. Chem.*, 2001, **22**, 931–967.
32 J. P. Perdew, K. Burke and M. Ernzerhof, *Phys. Rev. Lett.*, 1996, **77**, 3865–3868.
33 S. Grimme, S. Ehrlich and L. Goerigk, *J. Comput. Chem.*, 2011, **32**, 1456–1465.
34 E. van Lenthe, J. Snijders and E. Baerends, *J. Chem. Phys*, 1996, **105**, 6505–6516.
35 E. van Lenthe, R. van Leeuwen, E. J. Baerends and J. G. Snijders, *Int. J. Quantum Chem.*, 1996, **57**, 281–293.
36 E. van Lenthe, A. Ehlers and E. Baerends, *J. Chem. Phys.*, 1999, **110**, 8943–8953.
37 H.-Y. Cheng, P.-O. Åstrand, D. Chen, Y.-A. Zhu, X.-G. Zhou and P. Li, *Chem. Phys. Lett.*, 2013, **575**, 76–80.
38 M. Mahmoodinia, M. Ebadi, P.-O. Åstrand, D. Chen, H.-Y. Cheng and Y.-A. Zhu, *Phys. Chem. Chem. Phys.*, 2014, **16**, 18586–18595.
39 M. Mahmoodinia, P.-O. Åstrand and D. Chen, *J. Phys. Chem. C*, 2015, **119**, 24425–24438.
40 M. Mahmoodinia, P.-O. Åstrand and D. Chen, *J. Phys. Chem. C*, 2016, **120**, 12452–12462.
41 E. V. Lenthe and E. J. Baerends, *J. Comput. Chem.*, 2003, **24**, 1142–1156.
42 V. Fung and D.-E. Jiang, *J. Phys. Chem. C*, 2017, **121**, 10796–10802.
43 M. Mavrikakis and M. A. Barteau, *J. Mol. Catal. A: Chem.*, 1998, **131**, 135–147.
44 T. Watanabe, M. Ehara, K. Kuramoto and H. Nakatsuji, *Surf. Sci.*, 2009, **603**, 641–646.
45 A. L. Stottlemyer, H. Ren and J. G. Chen, *Surf. Sci.*, 2009, **603**, 2630–2638.
46 J. N. Bronsted, *Chem. Rev.*, 1928, **5**, 231–338.
47 R. P. Bell, *Proc. R. Soc. London, Ser. A*, 1936, **154**, 414–429.

48 M. G. Evans and M. Polanyi, *Trans. Faraday Soc.*, 1938, **34**, 11–24.
49 R. Alcalá, M. Mavrikakis and J. A. Dumesic, *J. Catal.*, 2003, **218**, 178–190.
50 D. Loffreda, F. Delbecq, F. Vigné and P. Sautet, *Angew. Chem. Int. Ed.*, 2009, **48**, 8978–8980.
51 R. A. van Santen, M. Neurock and S. G. Shetty, *Chem. Rev.*, 2010, **110**, 2005–2048.
52 S. Wang, V. Petzold, V. Tripkovic, J. Kleis, J. G. Howalt, E. Skúlason, E. M. Fernández, B. Hvolbæk, G. Jones, A. Toftelund, H. Falsig, M. Björketun, F. Studt, F. Abild-Pedersen, J. Rossmeisl, J. K. Nørskov and T. Bligaard, *Phys. Chem. Chem. Phys.*, 2011, **13**, 20760–20765.
53 J. E. Sutton and D. G. Vlachos, *ACS Catal.*, 2012, **2**, 1624–1634.
54 J. Zaffran, C. Michel, F. Auneau, F. Delbecq and P. Sautet, *ACS Catal.*, 2014, **4**, 464–468.